JOURNAL OF THERMOPHYSICS AND HEAT TRANSFER
Vol. 11, No. 2, April–June 1997

Viscous Flow of Plasmas on Nonequilibrium Thermodynamic Diagrams

Kuan Chen*
University of Utah, Salt Lake City, Utah 84112
and
Thomas L. Eddy†
MeltTran, Inc., Idaho Falls, Idaho 83401

Thermodynamic diagrams were developed for plasma flows not in local chemical equilibrium with viscous effects taken into consideration. Lines of constant mass flux were constructed on surfaces of zero affinity and constant composition to aid in understanding the transition process between equilibrium and frozen flows. Effects of friction on the changes in reaction extent and thermodynamic properties were studied for different mass fluxes and for both supersonic and subsonic flows. The relationship between the flow conditions and the duct length and friction factor of a viscous reacting flow is investigated. Two- and three-dimensional thermodynamic diagrams were constructed for singly ionized argon plasma at a stagnation state of 10 atm and 15,000 K. Use of the nonequilibrium diagrams for analyzing viscous reacting flows was illustrated in an example involving one-dimensional plasma flows through a supersonic nozzle with a constant-area duct attached to the nozzle exit.

Nomenclature

a = speed of sound
D_e = hydraulic diameter
e^- = free electron
F = chemical affinity
f = friction factor
G = mass flux, ρv
g_m = degeneracy of energy level m
H^0 = negative value of the heat of reaction
h = enthalpy
$\underline{h}$ = Planck's constant
K_p = equilibrium constant
k = Boltzmann's constant
k_b = reverse rate constant
L = length
m = mass
N = particle number
n = number density, $n_j = [j]$
p = pressure
R = gas constant
R = radiative recombination rate
s = entropy
T = temperature
v = velocity
X = mole fraction
x = length along the path of one-dimensional flow
Z = partition function
γ = specific heat ratio
Δh = enthalpy of formation
Δt = characteristic time
ε_m = energy of level m referred to the ground state
μ = chemical potential
ν = stoichiometric coefficient
$\underline{\nu}$ = frequency
ρ = density

Subscripts
chem = chemical energy or chemical reaction
e^- = free electron
g = ground state
j = species j
m, n = energy levels
t = translational energy mode
x = electronic excitation energy mode
0 = evaluated at the stagnation state

Superscripts
* = dimensionless quantities
0 = reference pressure

Received July 10, 1996; revision received Nov. 19, 1996; accepted for publication Nov. 19, 1996.

*Associate Professor, Department of Mechanical Engineering. Member AIAA.
†President. Member AIAA.

I. Introduction

REACTION rate calculations for plasmas are very difficult and tedious because of the numerous energy levels and energy exchange processes that must be taken into consideration in an ionization/recombination reaction. The difficulties and uncertainty in the determination of plasma reaction rates were discussed and demonstrated in many plasma texts and papers.[1–4] Rate coefficients for ionization and recombination reactions are often deduced from elaborate collisional–radiative models. Phelps[2] computed the collision cross sections of hydrogen plasma. Ionization and recombination rate coefficients for argon plasma at moderate to high degrees of ionization can be found in Ref. 4.

Repetti et al.[3] included 23 neutral argon excited states and seven chemical reactions in their chemical rate calculation for singly ionized argon atoms. Reaction rates for electron and heavy particle collisions were fit to Arrhenius and modified Arrhenius forms. Reverse reaction rates were determined by detailed balance. Repetti et al.[3] pointed out the spontaneous emission coefficients for neutral argon are accurate to only a factor of 2 to 5. Transitions between manifolds are therefore quite uncertain for chemical reaction calculation of argon plasmas.

Because accurate reaction rates for ionization/recombination reactions are very difficult to determine, nonequilibrium ther-

modynamic charts have been developed to aid in understanding the complex reactions involved and to predict the changes of composition and properties in plasma flows not in local chemical equilibrium. Since the state of a reacting flow is bounded by the states of frozen (zero reaction rate) and chemical equilibrium (infinite reaction rate) flows and the two limiting cases are, relatively speaking, simple to compute for plasmas, the solutions of equilibrium and frozen flows are often plotted on a nonequilibrium thermodynamic diagram as the boundaries of all the possible states of the reacting flow.

Frozen and equilibrium flow solutions have been applied to the analysis of reacting flows.[5,6] However, most of the previous reacting flow analyses only computed the frozen and equilibrium flows at one entropy value. It was pointed out by Chen and Eddy[7] that nonequilibrium charts of different entropy values are needed for the analysis of chemical reactions with finite reaction rates. Thermodynamic diagrams for nonequilibrium argon plasmas were constructed on planes of different entropy values in Chen and Eddy's[7] paper and applied to reacting flows through a supersonic nozzle.

The entropy of a flow may increase because of friction, heat addition, and finite rate chemical reactions. Although the nonequilibrium diagrams developed by Chen and Eddy[7] are applicable to any reacting flows (inviscid or viscous, adiabatic, or with heat transfer), since only thermodynamic properties are presented in these charts, attention in their previous investigation was focused on inviscid adiabatic flows in which only chemical reactions with finite reaction rates cause the entropy to increase. The states of an equilibrium or frozen flow without heat transfer or friction will lie on a plane of constant entropy. The equilibrium and frozen flow solutions presented on the planes of constant entropy are therefore useful to the analysis of reacting flows with negligible heat transfer and viscous effects. In a viscous flow without heat losses, the entropy increases continuously in the equilibrium and frozen flow regions. Therefore the isentropic flow simplification is not valid for viscous equilibrium or frozen flows. Nonequilibrium diagrams other than those constructed on constant entropy planes are needed when frictional effects must be taken into account.

In the present study the application of nonequilibrium thermodynamic diagrams is extended to reacting flows with frictional losses. Thermodynamic diagrams relevant to viscous flow analysis are developed and discussed. The effects of friction on the changes in reaction extent and plasma properties are investigated. The length of the flow channel and the friction factor are cast into a dimensionless parameter and computed for various reacting flows. An example of viscous reacting flows through a nozzle connecting to a constant-area duct is given to illustrate the use of the nonequilibrium viscous flow charts.

II. Nonequilibrium Thermodynamic Diagrams for Viscous Flows

The method for computing the equilibrium and frozen flow solutions of a reacting flow has been discussed in detail in the authors' previous publication.[7] The plasma considered in the present analysis is argon at a stagnation pressure of 10 atm and a stagnation temperature of 15,000 K. These stagnation properties are identical to those of the argon plasma considered in the authors' previous study of inviscid adiabatic flows. For argon plasmas below 20,000 K, the dominant reactions at moderate to high pressures are the formation and recombination of the singly ionized argon ions:

$$\mathrm{Ar} \leftrightarrow \mathrm{Ar}^+ + e^- \tag{1}$$

The chemical composition of argon plasma at p, T, and F can be determined from[8]

$$(1 - 2X_{e^-})/X_{e^-}^2 = (p^0/p)\exp[(F/(kT)]/K_p \tag{2}$$

where K_p is the equilibrium constant at p^0 and T, and X_{e^-} is the mole fraction of the free electrons. The affinity of a chemical reaction is defined as

$$F = -\sum \nu_j \mu_j \tag{3}$$

where ν_j and μ_j are the stoichiometric coefficient and chemical potential of species j, respectively. Positive values of F for the defining Eqs. (1) and (3) indicate either ionizing or underionized flows compared to chemical equilibrium ($F = 0$). Negative values indicate recombining or overionized flows. Chemical affinity has been commonly used in nonequilibrium thermodynamics as a measure of the degree of reaction extent.[9,10] Since change in affinity depends on the state of a thermodynamic system and is independent of the path by which the system arrived at the given state, affinity is a property of reacting flows. Thermodynamic tables or charts can be constructed at different affinity values for the analysis of flows not in local chemical equilibrium.[8,11,12]

With the chemical composition determined from Eq. (2), the density and specific enthalpy of argon plasma can be calculated from the following equations and thermodynamic relationships:

$$\rho = \sum m_j n_j \tag{4}$$

$$h = \sum m_j n_j h_j \tag{5}$$

where

$$h_j = h_{t,j} + h_{x,j} + h_{\mathrm{chem},j} \tag{6}$$

$$h_{t,j} = 2.5kT_{t,j} \tag{7}$$

$$h_{x,j} = kT_{x,j}Z'_{x,j}/Z_{x,j} \tag{8}$$

$$Z_{x,j} = \sum g_{xm} \exp[-\varepsilon_{xm}/(kT_{x,j})] \tag{9}$$

$$Z'_{x,j} = \sum g_{xm}[\varepsilon_{xm}/(kT_{x,j})]\exp[-\varepsilon_{xm}/(kT_{x,j})] \tag{10}$$

$$h_{\mathrm{chem},j} = 0 \quad \text{for} \quad j = \mathrm{Ar} \text{ and } e^-$$
$$h_{\mathrm{chem},j} = 2.5264 \times 10^{-19}\ \mathrm{kJ} \quad \text{for} \quad j = \mathrm{Ar}^+ \tag{11}$$

Just like enthalpy, the entropy of the argon plasma was calculated from the sum of the entropies of different species and energy modes:

$$s = \sum m_j n_j s_j \tag{12}$$

where

$$s_j = s_{t,j} + s_{x,j} \tag{13}$$

$$s_{t,j} = k[\ell n(Z_{t,j}/N_j) + 2.5] \tag{14}$$

$$s_{x,j} = k(\ell n\, Z_{x,j} + Z'_{x,j}/Z_{x,j}) \tag{15}$$

$$Z_{t,j}/N_j = (2\pi m_j/\underline{h}^2)^{3/2}(kT_{t,j})^{5/2}/p_j \tag{16}$$

For monatomic gases in LThE (local thermal equilibrium)

$$T_{t,j} = T_{x,j} = T \tag{17}$$

The electronic levels employed in the present calculation of argon composition and properties are those used in Sonntag and Van Wylen's book[13] for argon plasma around 10,000 K. The computed plasma properties for $T \leq 15{,}000$ K agree well with Sedghinasab and Eddy's[14] calculation of argon properties,

which included the first four argon ions and electronic energy levels up to 70.

The speed of sound for nonequilibrium argon plasmas was computed from

$$a = \left(\left. \frac{\partial p}{\partial \rho} \right|_s \right)^{0.5} \tag{18}$$

Small changes in p and ρ from a given state were evaluated along the constant entropy line, and the derivative of p with respect to ρ was approximated by the central difference scheme. A fixed chemical composition was assumed in the sound-speed calculation for frozen flows. The composition was determined from the zero affinity requirement when the sound-speed of equilibrium flow was calculated. The computed equilibrium sound-speed at low temperatures (temperatures at which the degree of ionization is almost negligible) agrees very well with the result of calorically perfect gases,[6] which can be expressed as

$$a = (\gamma RT)^{0.5} \tag{19}$$

Lines of constant mass flux are commonly employed in the analysis of viscous flows. A one-dimensional flow in a constant-area duct has constant mass flux, regardless of whether the flow is inviscid or viscous, reacting or frozen. The change in flow cross-sectional area is inversely proportional to the change in mass flux for one-dimensional steady flows. Thus, the effects of variable flow cross-sectional area can be investigated if constant mass flux lines of different values are constructed on thermodynamic diagrams. The equations for constant mass flux lines can be found in most gasdynamics texts for a calorically perfect gas. No equations are available for the constant mass flux lines of reacting flows in which both chemical composition and properties may change.

If the heat losses of a reacting flow are negligible, only thermodynamic diagrams above the stagnation entropy are needed since in this case the entropy of the flow will never decrease. Previous investigation of reacting flows by Chen and Eddy[7] showed that there also exists an upper limit for entropy if the minimum pressure is specified. Above this maximum entropy the enthalpy will be greater than the stagnation enthalpy. Consequently, only thermodynamic diagrams within a certain entropy range are needed to be constructed for a given stagnation state if the flow exchanges no heat and work with its surroundings.

To plot the constant mass flux line of a selected value on the zero affinity (chemical equilibrium) plane, a pressure was first picked and an entropy value guessed. The state of the reacting flow is defined by three independent properties: F (=0 on the equilibrium flow plane), p, and s. Other properties and the chemical composition at the state can be determined from these three properties and Eqs. (2-18). At first glance, it seems more convenient to guess T instead of s for property and composition calculations, since Eqs. (2-17) are explicit in T. However, a constant entropy process is required for the evaluation of the sound-speed. Therefore, s rather than T was selected as an independent property to fix the plasma state in the iterations.

The velocity was determined from the first-law equation:

$$h + v^2/2 = h_0 \tag{20}$$

The mass flux was calculated as the product of the density and the velocity. That is,

$$G = \rho v \tag{21}$$

A new entropy value was tried if the calculated mass flux was not very close to the selected value. After the correct entropy value was found by Newton's iteration, a new pressure was selected and the entropy iteration procedure was repeated until another point on the constant mass flux line was determined. Construction of the constant mass flux line continues until a complete curve was plotted on the zero affinity plane.

Construction of constant mass flux lines on a surface of constant chemical composition was carried out in a similar manner. The only differences are that the composition was fixed and that the affinity at each point on the constant composition surface must be calculated from Eq. (2). Strictly speaking, the composition of a viscous flow may change via diffusion even though the flow is chemically frozen.[6] However, the differences between equilibrium and chemically frozen flows are smaller than those between equilibrium and completely frozen (chemically frozen plus zero diffusion rate) flows. Therefore, the state of a viscous flow with zero reaction rates will fall within the bounds of equilibrium and frozen (constant composition) flows.

Single precision with seven-digit accuracy was employed in our calculations. The pressure increments used in the sound-speed calculation were approximately one-hundredth of the plasma pressure. The convergence criterion for entropy iteration was chosen to be

$$\left| s_{\text{calculated}} - s_{\text{assigned}} \right| / s_{\text{assigned}} \leq 10^{-6} \tag{22}$$

This small convergence criterion was used to ensure good accuracy for thermodynamic property calculations. After entropy iteration converged, the mass flux was computed from Eqs. (20) and (21). If the difference between the calculated and desired mass fluxes was not very small, a new entropy value was assigned and the double iteration procedure continued. The convergence criterion for mass flux iteration was

$$\left| G_{\text{calculated}} - G_{\text{desired}} \right| / G_{\text{desired}} \leq 10^{-2} \tag{23}$$

The use of a relatively large convergence criterion for mass flux iteration is because the accuracy for thermodynamic property calculations varies as the square of the accuracy for velocity calculation, as shown in Eq. (20). If too small a convergence criterion was selected for mass flux iteration, the convergence criterion for entropy iteration should be much smaller and the property calculations very time consuming.

III. Results and Discussion

Several two-dimensional diagrams of the constant mass flux lines were constructed and presented in Figs. 1-6 for equilibrium flow ($F = 0$) and two frozen flows ($X_{e^-} = 0.1$ and 0.2). F^* in these diagrams is the dimensionless affinity: F divided by the negative value of the heat of reaction at 0 K. That is,

$$F^* = F/H^0 \tag{24}$$

where

$$H^0 = -\sum \nu_j \Delta h_j \tag{25}$$

Two three-dimensional diagrams are also presented in Figs. 7 and 8 to aid in understanding the changes in reaction extent and entropy for various reacting flows. These diagrams were developed for argon plasma at a stagnation state of $p_0 = 10$ atm and $T_0 = 15{,}000$ K. The degree of ionization at the stagnation state is $X_{e^-,0} = 0.182$. Therefore, frozen flow solutions for $X_{e^-} = 0.1$ and 0.2 were computed. Frozen flows of other compositions can be estimated from interpolation or extrapolation of these two frozen flow results.

Whether a chemically reacting flow can be treated as an equilibrium or frozen flow depends on the value of the Damkohler number. The Damkohler number is the ratio of the characteristic flow time to the characteristic time of the chemical reaction.[15,16] A very small Damkohler number implies that the

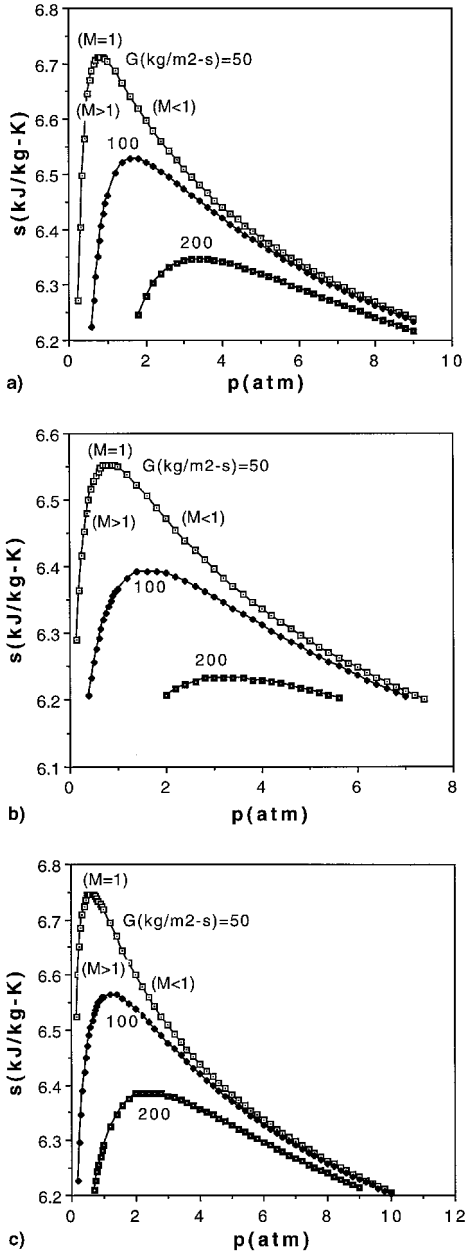

Fig. 1 Pressure–entropy diagram of constant mass flux processes: a) equilibrium flow, $F^* = 0$; b) frozen flow, $X_{e^-} = 0.1$; and c) frozen flow, $X_{e^-} = 0.2$.

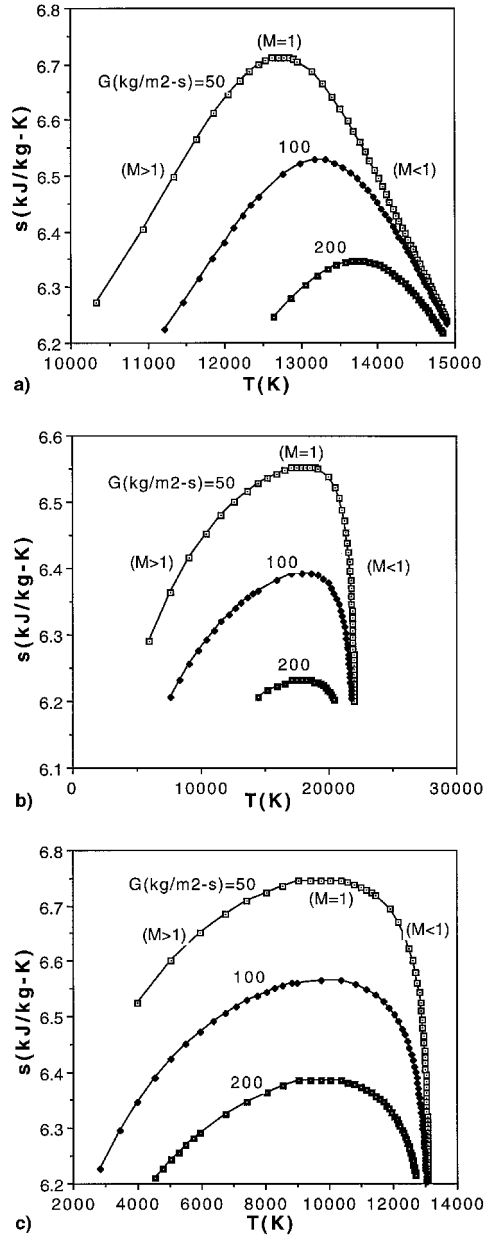

Fig. 2 Entropy–temperature diagram of constant mass flux processes: a) equilibrium flow, $F^* = 0$; b) frozen flow, $X_{e^-} = 0.1$; and c) frozen flow, $X_{e^-} = 0.2$.

effect of chemical reaction on the flow is negligible and the flow is chemically frozen. At the other extreme, the flow can be assumed to be in local chemical equilibrium if the Damkohler number is very large.[15] For a one-dimensional flow, the characteristic flow time is the characteristic length in the flow direction (e.g., the length of a nozzle or a duct) divided by the average flow velocity.

The characteristic time of a plasma reaction is very cumbersome and difficult to estimate. Not only a large number of energy levels and various chemical reactions must be taken into consideration, but the accuracy of the reaction rate coefficients of these reactions are quite uncertain.[3] If the kinetic model for argon plasma developed by Repetti et al.[3] is employed, the reactions associated with the recombination of singly ionized argon plasma are the radiative recombination:

$$Ar^+ + e^- \rightarrow Ar_n + \underline{h\nu} \tag{26}$$

and the reverse reactions of the ionization reactions involving collisions between electrons and argon atoms:

$$Ar_m + Ar_g \leftrightarrow Ar^+ + Ar_g + e^- \tag{27}$$

$$Ar_m + e^- \leftrightarrow Ar^+ + e^- + e^- \tag{28}$$

where the subscripts m and n denote neutral argon energy levels and state m lies below state n. The ground-state argon atoms are denoted by the subscript g. The reverse reactions of Eqs. (27) and (28) involve collisions of three particles. The frequencies of these three-body collisions should be much lower than that of the two-body collision shown in Eq. (26) for low-temperature argon plasmas. If only the reaction in Eq. (24) is considered, the generation rate of Ar_n can be expressed as

$$\frac{d[Ar_n]}{dt} = R_n[Ar^+][e^-] \tag{29}$$

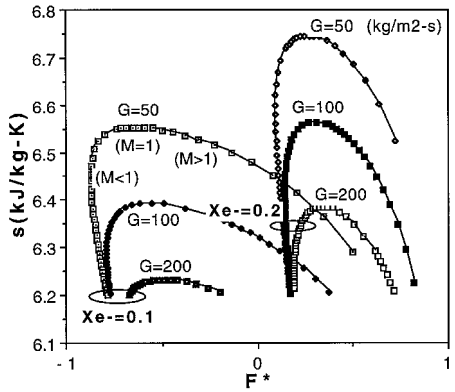

Fig. 3 Affinity–entropy diagram of constant mass flux processes.

where R_n is the radiative recombination rate to level n of neutral argon. The numerical value of R_n was found to be between 10^{-19} and $4 \times 10^{-21} T_e^{-0.5}$ m^3/s.[3,17,18] The generation rate of argon atoms of all levels in a recombination reaction can be estimated based on the fastest reaction. Thus,

$$\frac{\mathrm{d}[\mathrm{Ar}]}{\mathrm{d}t} = k_b[\mathrm{Ar}^+][e^-] \tag{30}$$

where the reverse rate constant is about $10^{-19} T_e^{-0.5}$ m^3/s. For plasmas in local thermal equilibrium, $T_e = T$.

For the recombination of Ar^+ and e^-, the time required for the reacting flow from a nonequilibrium state to reach the equilibrium state can be estimated from the integration of Eq. (30). The result is

$$[\mathrm{Ar}]_{\mathrm{final}} - [\mathrm{Ar}]_{\mathrm{initial}} = \Delta t_{\mathrm{chem}} k_{b,\mathrm{mean}} [\mathrm{Ar}^+]_{\mathrm{mean}} [e^-]_{\mathrm{mean}} \tag{31}$$

For a small time interval Δt, the mean values of k_b, $[Ar^+]$, and $[e^-]$ in the previous equation should be between the initial and final values. Therefore, if the initial concentrations of the recombination reaction are known, the chemical reaction time constant can be estimated from

$$[[\mathrm{Ar}]_{\mathrm{final}} - [\mathrm{Ar}]_{\mathrm{initial}}]/[\, k_{b,\mathrm{initial}} [\mathrm{Ar}^+]_{\mathrm{initial}} [e^-]_{\mathrm{initial}}] \le \Delta t_{\mathrm{chem}}$$
$$\le [[\mathrm{Ar}]_{\mathrm{final}} - [\mathrm{Ar}]_{\mathrm{initial}}]/[\, k_{b,\mathrm{final}} [\mathrm{Ar}^+]_{\mathrm{final}} [e^-]_{\mathrm{final}}] \tag{32}$$

The final concentrations in the previous equation are the equilibrium concentrations. With the flow and chemical reaction time constants estimated, the local Damkohler number can be calculated to determine if the flow is chemically frozen or in chemical equilibrium.

If the forward and reverse reaction coefficients of all the reactions involved are known, the local plasma temperature(s) and species concentrations can be calculated for a reacting flow. This information is needed for the estimation of the reaction time constant. The results, however, are only valid for one particular flow. When the nozzle angle, duct or nozzle length, or friction coefficient of the flow changes, the local flow conditions will change and a new reacting flow calculation must be carried out to determine the reaction time constant.

The chemical reaction time constant can also be estimated from the measurements of local plasma properties. For instance, if T and p were measured to be 8000 K and 0.2 atm for a duct flow at $G = 50$ kg/m^2-s, the corresponding entropy values in Fig. 1 at the measured p would be approximately 6.27, 6.4, and 6.65 kJ/kg-K for $F^* = 0$, $X_e = 0.1$, and 0.2, respectively. Entering these entropy values and $G = 50$ kg/m^2-s into the s–T diagrams in Fig. 2, it can be seen that only the supersonic solution for $X_e = 0.1$ yields $T = 8000$ K. Thus, the

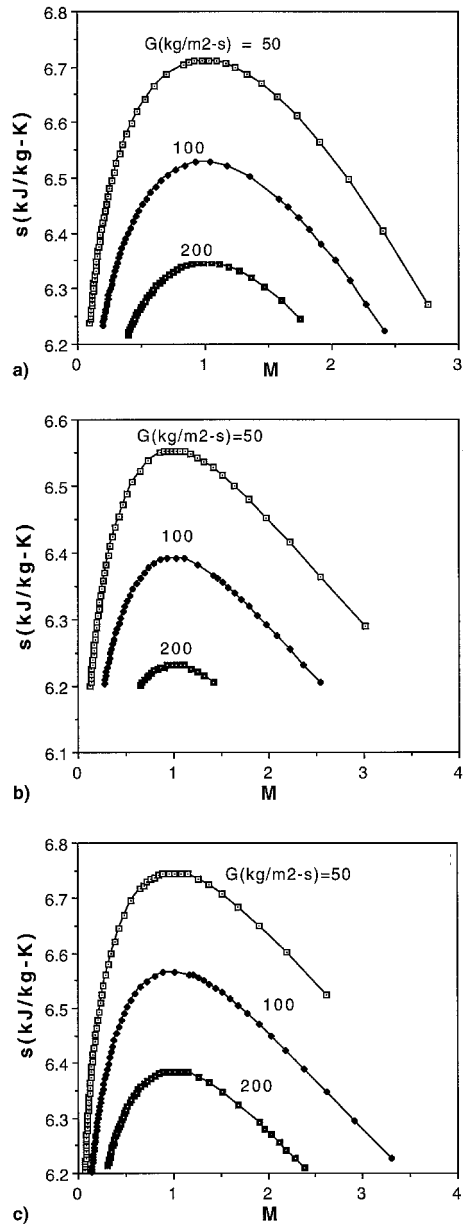

Fig. 4 Mach number–entropy diagram of constant mass flux processes: a) equilibrium flow, $F^* = 0$; b) frozen flow, $X_e = 0.1$; and c) frozen flow, $X_e = 0.2$.

entropy and chemical composition of the argon plasma would be $s = 6.4$ kJ/kg-K and $X_e = 0.1$, respectively. The other properties then could be determined from the frozen flow charts for $X_e = 0.1$ at $s = 6.4$ kJ/kg-K. For the same G and p values, the equilibrium plasma temperature and concentrations could be determined from Figs. 1a, 2a, and 5a. Thus, all of the information needed for the Δt_{chem} calculation could be obtained. If the characteristic length of the flow were specified, Δt_{flow} could be estimated from Fig. 6b and the Damkohler number could be determined.

The effects of friction on the reacting flow of argon plasma are now discussed. As shown in the F^*–s–p diagram in Fig. 7, frozen flow surfaces of lower X_e are enclosed by surfaces of higher X_e. Thus, X_e may be higher than $X_{e,0}$ if the increase in X_e caused by friction is greater than the decrease in X_e because of the temperature drop in an accelerating flow (e.g., process a–c in Fig. 7). However, the calculated p–s diagrams (Figs. 1a–1c) show a very slow entropy increase as p decreases in viscous subsonic flows ($M < 1$). Thus an X_e greater than $X_{e,0}$ seems very unlikely for argon plasmas in the temperature and pressure ranges we considered.

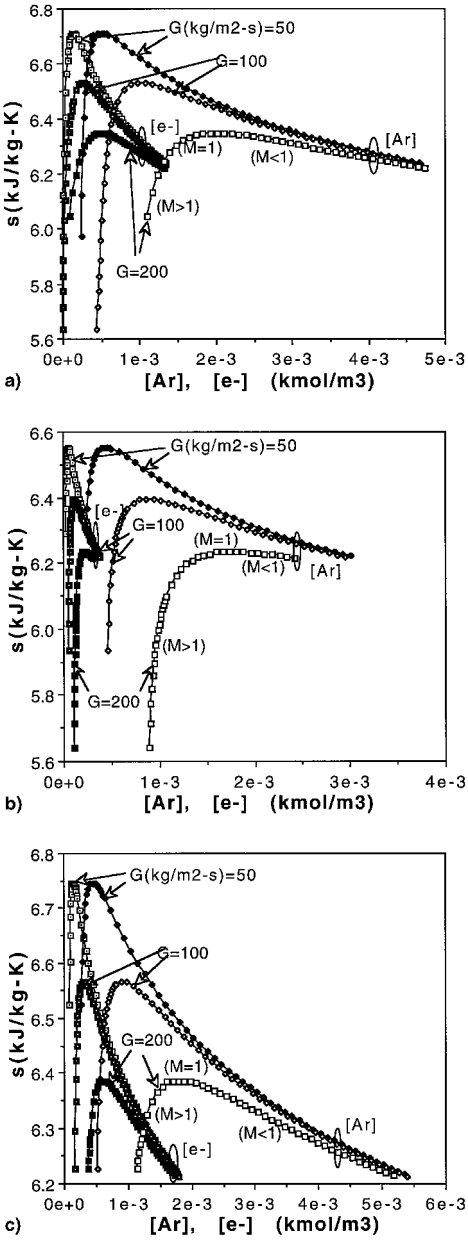

Fig. 5 Concentration–entropy diagram of constant mass flux processes: a) equilibrium flow, $F^* = 0$; b) frozen flow, $X_{e^-} = 0.1$; and c) frozen flow, $X_{e^-} = 0.2$.

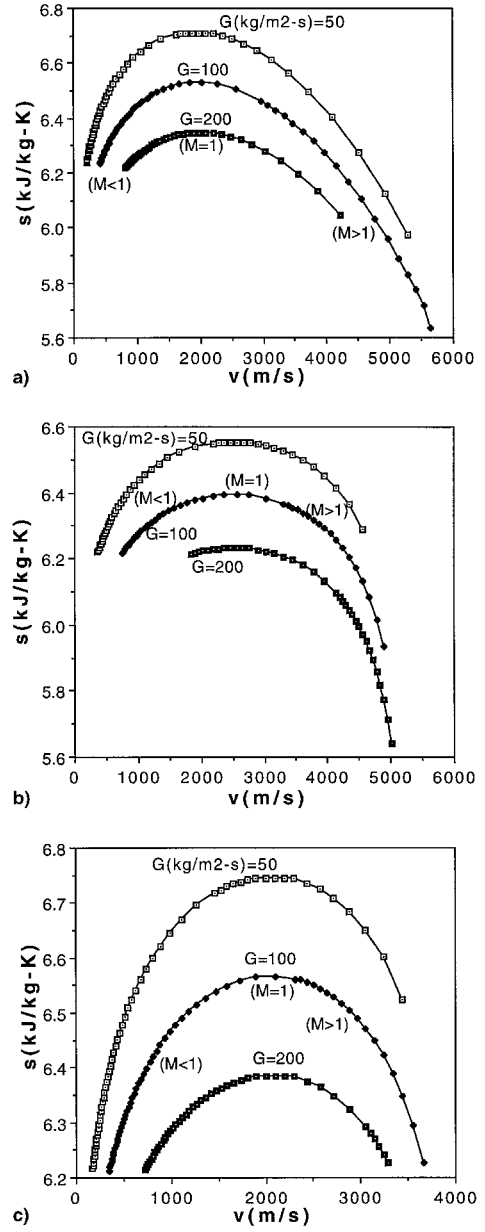

Fig. 6 Velocity–entropy diagram of constant mass flux processes: a) equilibrium flow, $F^* = 0$; b) frozen flow, $X_{e^-} = 0.1$; and c) frozen flow, $X_{e^-} = 0.2$.

The $p-s$ diagrams in Figs. 1a–1c show that the pressure at $M = 1$ decreases as G decreases. On the contrary, the maximum entropy, which occurs at $M = 1$, increases as G decreases for both equilibrium and frozen flows. If only frozen flows with $X_{e^-} < X_{e^-,0}$ are considered, the maximum entropy of equilibrium flow is always greater than that of frozen flows of identical G. These plots also indicate that for a given stagnation entropy, there exists a maximum G the flow can reach if heat losses are negligible (s always increases in this case). The maximum mass flux of equilibrium flow is higher than those of frozen flows with $X_{e^-} < X_{e^-,0}$.

The $s-T$ diagrams presented in Figs. 2a–2c show that the temperature at $M = 1$ increases as the mass flux increases in equilibrium flow, but does not vary much with G in frozen flows. Pressure, temperature, and entropy all increase when an equilibrium or frozen flow of constant G is decelerated from supersonic to sonic flow (see the branches of $M \geq 0$ in Figs. 1 and 2). The $h-s$ diagrams are very similar to the $s-T$ diagrams and are therefore not presented.

The F^*-s plots of two frozen flows (Fig. 3) show similar affinity dependence on G and M. F^* first decreases as M decreases. At very low Mach numbers, however, F^* starts to increase as M decreases. Change in frozen flow composition has significant effects on the range of affinity variation. For flows frozen at high degrees of ionization (e.g., $X_{e^-} = 0.2$ in Fig. 3), both the supersonic and subsonic flow branches of the constant G lines are mainly in the region of positive F^*, indicating the X_{e^-} of the frozen flow is higher than that of the equilibrium flow at the same T and p. As X_{e^-} decreases, the affinity–entropy diagram of constant G lines moves into the negative F^* territory and has a smaller range of entropy variation. Thus, for the flows frozen at low degrees of ionization (e.g., $X_{e^-} = 0.1$ in Fig. 3), F^* is positive only at high M and low G.

Figure 3 is interesting because it shows both positive and negative F^* values. For the $X_{e^-} = 0.2$ case, the F^* values are all positive, indicating that these flow states are all recombining (or are overionized for the local temperature). For the $X_{e^-} = 0.1$ case, the F^* values are mostly negative, except at

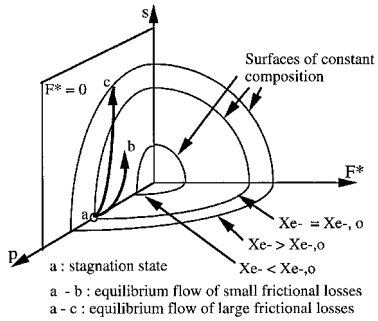

Fig. 7 Surfaces of constant composition on the affinity–pressure–entropy diagram.

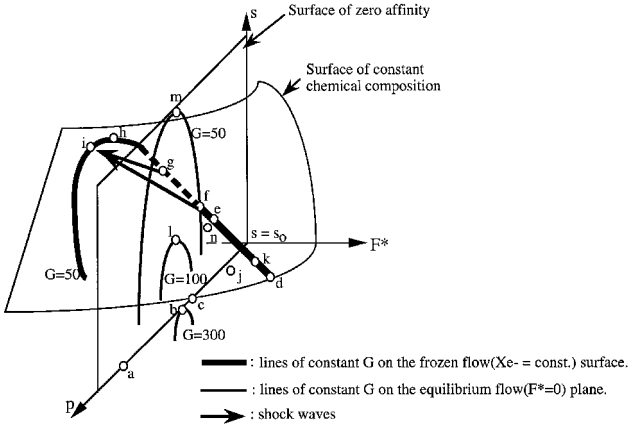

Fig. 8 Various reacting flow processes on the affinity–pressure–entropy diagram.

very high Mach numbers. The negative F^* values indicate that the flow states in the $M > 1$ region, that should be in a recombining phase, are actually ionizing because of the viscous heating. This region is underionized because the degree of ionization is not keeping up with that corresponding to equilibrium with viscous heating. At the higher degree of ionization (X_e- = 0.2), the viscous heating is insufficient to raise the temperature above that corresponding to the equilibrium temperature and recombination prevails throughout. This is not the case for X_e- = 0.1, where the viscous heating raised the temperature above the equivalent equilibrium temperature and the plasma is underionized.

The effects of friction on the deviation from chemical equilibrium (measured by the absolute value of F^*) are opposite in subsonic and supersonic frozen flows. Consider a supersonic frozen flow entering an insulated duct of constant area with G = 100 kg/m^2-s and a composition of X_e- = 0.2. Figure 3 indicates the deviation from chemical equilibrium will decrease as the flow is decelerated to sonic speed. On the other hand, if a subsonic frozen flow of identical G and X_e- enters the duct, its F^* and M will both increase (except for F^* at very low M) because of friction and the deviation from chemical equilibrium will increase.

The information most useful to viscous flow analysis is the relationship between the duct length and friction factor and the flow conditions. For one-dimensional flows with negligible change in potential energy, the momentum equation is[19]

$$\frac{dp}{\rho} + fv^2 \frac{dx}{(2D_e)} + \frac{d(v^2)}{2} = 0 \qquad (33)$$

Equation (33) can be rearranged as

$$f\frac{dx}{D_e} = -2\left[\frac{dp}{\rho} - \frac{d(v^2)}{2}\right] \Big/ v^2 \qquad (34)$$

Equation (34) was integrated numerically along the lines of constant G. The results are presented in Figs. 9 and 10. The dimensionless parameter fL/D in these figures is the integration of $f(dx/D_e)$ from a point on a constant G line to the point of $M = 1$ on the same constant G line.

Application of the fL/D diagrams to viscous flow analysis is very straightforward if f is constant. The required duct length or friction factor for a particular flow state can be easily determined from these diagrams. In a reacting flow, however, f may not be constant because of the change in chemical composition. In this case the integration of $f(dx/D_e)$ can still be performed if the relationship between f and v can be determined. Furthermore, Eq. (34) can be integrated for flows with variable area if the variation of D_e with x is specified.

The plot of M vs fL/D (Fig. 9) shows that the relationship between fL/D and M is independent of G. This is identical to that of calorically perfect gases. The lines of equilibrium and frozen flows almost coincide for $M < 1$. Only at large M can the difference among the three flow results in Fig. 9 be seen. The results of calorically perfect gases also show very week dependence of specific heat ratio for M near unity. The observation that the Mach number – fL/D relation is independent of G and only weakly dependent on reaction extent makes it easy to determine the duct dimensions or the friction factor for a given Mach number if M is not much greater than unity. It should be kept in mind, however, that the speed of sounds for different reacting flows are different. The gas velocities of equilibrium flow and frozen flows of different compositions are different at the same Mach number. Thus, the Mach number is not a particularly useful quantity for nonequilibrium flows, as pointed out by Anderson.[6]

The shapes of the constant G lines on the fL/D–s diagrams (Figs. 10a–10c) are very similar. The parameter fL/D decreases as s increases for both supersonic and subsonic flows. Supersonic flows have much smaller fL/D than subsonic flows. Since flows of lower G have higher s, the constant G lines shift vertically upward as G decreases. Except for slight differences in entropy, the fL/D–s diagrams for equilibrium flow and frozen flows with X_e- between 0.1–0.2 are very similar to one another. Combining Fig. 10 with Figs. 1 and 2, the required duct length or friction factor for a given T or p can be estimated.

The previous nonequilibrium diagrams are now applied to an example of one-dimensional reacting flow. In this example, argon plasma at p_0 = 10 atm and T_0 = 15,000 K is discharged through a convergent–divergent nozzle connecting to a duct of constant area. If the flow through the nozzle can be simplified to be isentropic, then friction and heat losses are negligible and the transition from equilibrium to frozen flow takes place abruptly. This nozzle flow can be represented by the

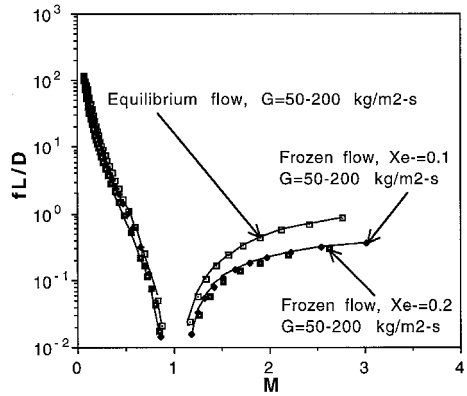

Fig. 9 fL/D–Mach number diagram for reacting flows of different G.

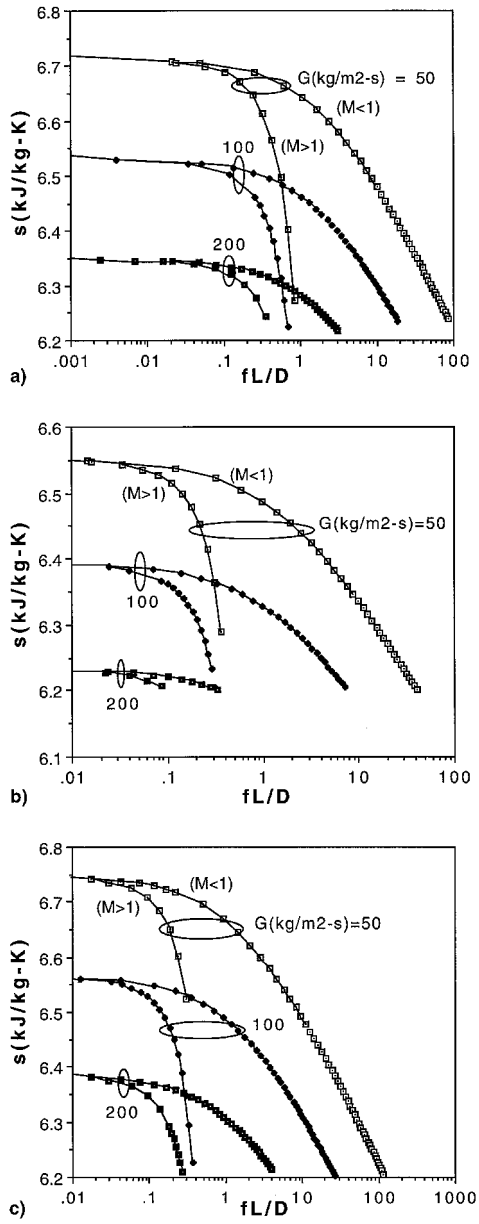

Fig. 10 ***fL/D*-entropy diagram of constant mass flux processes: a) equilibrium flow, $F^* = 0$; b) frozen flow, X_e- = 0.1; and c) frozen flow, X_e- = 0.2.**

isentropic process *a*–*b*–*c*–*d*, which lies on the plane of s = const = s_0 in Fig. 8.

As discussed in Chen and Eddy's previous publication,[7] an abrupt transition from equilibrium to frozen flow can only occur in an idealized nozzle that has a very large nozzle angle and the accelerating flow can follow the nozzle contour perfectly. If chemical reactions with finite reaction rates occur, but heat transfer and viscous effects are still negligible, the flow through the nozzle should resemble the process *a*–*b*–*j*–*k* in Fig. 8. States *j* and *k* are on the same frozen flow surface and have identical entropy. Notice that the equilibrium (*a*–*b*) and frozen (*j*–*k*) flows are isentropic, but lie on different constant entropy planes because of the increase in entropy associated with finite reaction rates in the process from state *b* to state *j*.

The nozzle flow with viscous effects included is represented by process *a*–*l*–*n*–*e* in Fig. 8. The flow velocity is generally low and the pressure is high in the convergent portion of a supersonic nozzle.[20] Thus, deviation from chemical equilibrium is small in process *a*–*l* and the plasma state remains on the zero affinity plane. However, the effects of viscosity cause the entropy to increase. This causes the sonic flow ($M = 1$) to occur at a lower G value when compared to the inviscid flow (process *a*–*b*). Between equilibrium and frozen flows is the region in which reactions of finite reaction rates take place. Entropy increases in this region because of both finite reaction rates and frictional losses (i.e., $s_n > s_l$). After the flow is frozen, the state of the plasma lies on a surface of constant composition, but the entropy continuously increases because of friction (i.e., $s_e > s_n$). Since the constant composition surface is inclined to the three axes of the F^*–s–p diagram in Fig. 8, the higher the entropy, the smaller the range of affinity variation will be.

The flow in the constant-area duct is now discussed. If the flow entering the duct is frozen and its G, p, and T can be measured at the duct inlet (p and T are relatively easy to measure; G can be computed from the mass flow rate divided by the duct area), the composition and properties of the flow at the duct entrance can be determined from Figs. 1–6. For instance, if the inlet conditions of argon plasma were measured to be G = 50 kg/m^2-s, p = 0.2 atm, T = 8000 K, the other properties and composition determined from the frozen flow charts would be approximately s = 6.4 kJ/kg-K, X_e- = 0.1, F^* = 0.25, M = 2.3. Because of the high Mach number and the low temperature, the frozen flow assumption is justified.

Since the duct cross-sectional area remains unchanged, the state of the plasma flow in the duct will be on the lines of G = 50 kg/m^2-s. If the flow in the duct does not remain frozen, its state will move to the lines of G = 50 kg/m^2-s on the frozen flow surfaces closer to the equilibrium flow plane. Eventually the state of the reacting flow will reach the line of G = 50 kg/m^2-s on a frozen flow surface so close to the equilibrium flow plane that the difference between frozen and equilibrium flows becomes negligible. Transition back to equilibrium flow is completed and from there the flow will follow the G = 50 kg/m^2-s line on the zero affinity plane.

Because frozen flow surfaces of smaller X_e- are enclosed by those of larger X_e- on the F^*–p–s diagram, a reacting duct flow with finite reaction rate starting at state *d* in Fig. 8 would follow a process below the frozen flow process *d*–*k*–*e*–*f* unless friction causes more ionization than recombination of the argon plasma. If the effect of recombination reaction dominates, the flow of finite reaction rate will reach the plane of zero affinity at a point below state *f* on the line of G = 50 kg/m^2-s. After reaching the zero affinity plane, the chemical reaction rate of the flow becomes very large and the flow will follow the equilibrium flow solution of G = 50 kg/m^2-s. As the heat generated by friction causes more argon atoms to ionize, the composition becomes identical to that at the duct inlet (state *d*) when the equilibrium flow reaches state *f* on the F^*–p–s diagram in Fig. 8.

If the flow in the duct remains frozen, the plasma state will follow the line of G = 50 kg/m^2-s on a frozen flow surface, as indicated by the frozen flow process *d*–*k*–*e*–*f* in Fig. 8. The line of G = 50 kg/m^2-s on the frozen flow surface intersects with the constant G line of the same value on the equilibrium flow plane at point *f*. This implies that because of the increase in temperature in a viscous duct flow, the compositions of the frozen and equilibrium flows become identical at point *f*. But since the flow at point *f* is still too fast to allow sufficient collisions for chemical equilibrium, the flow after point *f* remains on the frozen flow surface and its F^* becomes negative. A negative F^* implies the frozen flow composition has a lower degree of ionization than that of an equilibrium flow at the same temperature and pressure. This is the consequence of the large temperature increase caused by significant frictional losses. The temperature increase in equilibrium would increase the degree of ionization, but in nonequilibrium the state can appear to be underionized rather than to be recombining in this duct because of the viscous heating effect.

If the plasma flow enters the duct at $M > 1$ and the duct is very long and well insulated, transition from supersonic to sub-

sonic flow cannot pass the sonic state since the entropy must always increase in a viscous adiabatic flow. A shock wave will occur that causes the state of the flow to jump from the supersonic to the subsonic branch of a constant G line. The flow immediately after the shock is frozen. The shock will therefore occur on a frozen flow (constant composition) surface. The process g–i in Fig. 8 represents a shock wave in the frozen flow. If transition from supersonic to subsonic flow occurs in an equilibrium flow, the state of the flow after the shock will be on the line of the same G on a frozen flow surface passing through the equilibrium flow state before the shock. The process f–i in Fig. 8 represents a shock wave occurring at state f in an equilibrium flow.

As the flow is slowed down considerably after the shock, transition back to equilibrium flow may occur and the entropy will increase because of both friction (s increases from i to h if the flow remains frozen) and transition from frozen to equilibrium flow (entropy at m is greater than that at h). If the duct is very long, the flow is sonic at the duct exit and the ranges of exit T and p can be determined from Figs. 1a and 1b and 2a and 2b for $M = 1$ and $G = 50$ kg/m^2-s.

The complete frozen flow discussed earlier is the limiting case of chemically frozen viscous flows. If the flow is chemically frozen but composition changes because of diffusion, the state of the plasma will move closer to the zero affinity plane. As the frozen flow surfaces in Fig. 7 indicate, the effect of diffusion causes the chemically frozen flow to move to the surfaces of lower X_e- if F^* is positive, or to the surfaces of higher X_e- if F^* is negative.

IV. Conclusions

Equilibrium and frozen flow solutions were constructed on nonequilibrium thermodynamic diagrams for analyzing viscous reacting flows. The lines of constant mass flux on the equilibrium and frozen flow diagrams are in general similar to those of nonreacting flows of constant properties. The entropy of the constant mass flux lines decreases as the mass flux increases. The maximum entropy of a constant mass flux line always occurs at unit Mach number for both equilibrium and frozen flows. The relation between the parameter fL/D and the Mach number for viscous reacting flows is independent of the mass flux and only weakly dependent on the reaction extent. Except for very low Mach numbers, the dimensionless affinity increases as the Mach number increases. The effects of friction on the deviation from chemical equilibrium are opposite in subsonic and supersonic flows. Thus, if viscous effects cause a frozen flow to deviate further from equilibrium before a shock, the same effects will bring the frozen flow state back toward chemical equilibrium after the shock.

References

[1]Griem, H. R., *Plasma Spectroscopy*, McGraw–Hill, New York, 1964.

[2]Phelps, A. V., "Cross Sections and Swamp Coefficients for H^+, H_2^+, H_3^+, H, H_2, and H^- in H_2 for Energies from 0.1 eV to 10 kev," *Journal of Physical and Chemical Reference Data*, Vol. 19, No. 3, 1990, pp. 653–675.

[3]Repetti, T. E., Fincke, J. R., and Neuman, W. A., "Relaxation Kinetics of Argon Thermal Plasmas," *Heat Transfer in Thermal Plasma Processing*, HTD — Vol. 161, American Society of Mechanical Engineers, New York, 1991, pp. 167–176.

[4]Lelevkin, V. M., Otorbaev, D. K., and Schram, D. C., *Physics of Non-Equilibrium Plasmas*, North-Holland, Amsterdam, The Netherlands, 1992, pp. 313–409.

[5]Sutton, G. P., *Rocket Propulsion Elements*, 5th ed., Wiley, New York, 1986, pp. 131–144.

[6]Anderson, J. D., *Modern Compressible Flow*, 2nd ed., McGraw–Hill, New York, 1990, pp. 17–616.

[7]Chen, K., and Eddy, T. L., "Thermodynamic Charts for Non-Equilibrium Plasma Flow in a Supersonic Nozzle," *Journal of Thermophysics and Heat Transfer*, Vol. 10, No. 1, 1996, pp. 155–161.

[8]Chen, K., and Eddy, T. L., "Investigation of Chemical Affinity for Reacting Flows of Non-LThE Gases," *Journal of Thermophysics and Heat Transfer*, Vol. 9, No. 1, 1995, pp. 41–46.

[9]De Donder, T., and Van Rysselberghe, P., *Thermodynamic Theory of Affinity*, Stanford Univ. Press, Stanford, CA, 1936, p. 34.

[10]Haase, R., *Thermodynamics of Irreversible Processes*, Addison–Wesley, Reading, MA, 1969, p. 39.

[11]Chen, K., and Eddy, T. L., "Composition and Partition Functions of Partially Ionized Hydrogen Plasma in Non-Local Thermal Equilibrium and Non-Local Chemical Equilibrium," *Journal of Nonequilibrium Thermodynamics*, Vol. 18, No. 1, 1993, pp. 1–18.

[12]Chen, K., and Eddy, T. L., "Thermodynamic Properties of Molecular Hydrogen Plasma in Thermal and Chemical Nonequilibrium," *Journal of Thermophysics and Heat Transfer*, Vol. 7, No. 2, 1993, pp. 277–284.

[13]Sonntag, R. E., and Van Wylen, G. J., *Fundamentals of Statistical Thermodynamics*, Wiley, New York, 1966, pp. 262, 263.

[14]Sedghinasab, A., and Eddy, T. L., "Nonequilibrium Thermodynamic Properties of Argon," *Heat Transfer in Thermal Plasma Processing*, HTD — Vol. 161, American Society of Mechanical Engineers, New York, 1991, pp. 187–193.

[15]Kuo, K. K., *Principles of Combustion*, Wiley, New York, 1986, pp. 661–663.

[16]Rosner, D. E., *Transport Processes in Chemically Reacting Flow Systems*, Butterworths, London, 1986, pp. 321–443.

[17]McWhirter, R. W. P., "Spectral Intensities," *Plasma Diagnostic Techniques*, edited by R. H. Huddlestone, and S. L. Leonard, Academic, New York, 1965, p. 210.

[18]Bacri, J., Gomes, A. M., and Benzaid, S., "Etude des Ecarts al'etl dans un arc d'Argon (p=760 Torr)," *Journal of Physics D: Applied Physics*, Vol. 9, 1976, pp. 1743–1755.

[19]Zucker, R. D., *Fundamentals of Gas Dynamics*, Matrix Publishers, Chesterland, OH, 1977, pp. 235–265.

[20]Pierce, F. J., *Microscopic Thermodynamics*, International Textbook, London, 1968, pp. 364–367.